Lifetime measurements in the yrast band of ^{212}Po with a shell-model investigation

V. Karayonchev,[1,2,*] G. Rainovski,[1] J. Jolie,[2] A. Blazhev,[2] A. Dewald,[2] A. Esmaylzadeh,[2] C. Fransen,[2] P. John,[3] L. Knafla,[2] D. Kocheva,[1] K. Schomacker,[2] V. Werner,[3] and H. Naïdja[4]

[1]*Faculty of Physics, St. Kliment Ohridski University of Sofia, 1164 Sofia, Bulgaria*

[2]*Institut für Kernphysik, Universität zu Köln, 50937 Köln, Germany*

[3]*Institut für Kernphysik, Universität Darmstadt, 64289 Darmstadt, Germany*

[4]*Université Constantine 1, Laboratoire de Physique Mathématique et Subatomique, Constantine 25000, Algeria*

(Received 15 October 2021; accepted 28 November 2022; published 7 December 2022)

The lifetimes of the first excited 4^+ and 6^+ states in ^{212}Po were measured using the recoil-distance Doppler shift method. The nucleus of interest was populated in the ^{208}Pb(^{18}O, ^{14}C)^{212}Po reaction. The experimental results are compared to large-scale shell model calculations performed using the recently developed H208 effective interaction. The calculations describe well the low-lying structure of ^{212}Po with an exception of the $2_1^+ \rightarrow 0_1^+$ transition rate which is strongly overestimated. This has been attributed to additional components in the wave function of the ground state.

DOI: 10.1103/PhysRevC.106.064305

I. INTRODUCTION

The shell model is one of the most successful models of the atomic nucleus. In this model, the individual nucleons move in an external potential, a mean-field that is created by all the other nucleons. The addition of a spin-orbit term in the interaction allows the reproduction of the magic number which corresponds to closed major shells [1]. In opened-shell nuclei, the valence nucleons, those above the closed shell, interact with each other with a two-body residual interaction. This interaction is usually derived from realistic nucleon-nucleon potentials. Such are the approach of Kuo and Herling [2] based on the Hamada-Johnson potential [3] and the $V_{\text{low-}k}$ approach [4,5] derived from realistic potentials such as the Bonn [6], N3LO [7], and Argonne [8]. The number of possible configurations grows rapidly as the number of valence nucleons is increased. Even with modern supercomputers, the maximum number of valence nucleons for which shell model calculations can be performed remains limited. In this context nuclei with only a few valence nucleons play an important role in the construction and testing of the shell model interaction. The calculations for them could be performed in a large basis without the need for truncations which could obscure the interpretation of the results.

Nuclei in the vicinity of the heaviest stable doubly magic nucleus ^{208}Pb have attracted significant experimental and theoretical interest. Experimentally, the nuclei around the stable ^{208}Pb could be accessed relatively easily and there is a large amount of spectroscopic data already available. The fact that ^{208}Pb has a good doubly magic character has motivated many shell-model calculations [9–13]. These calculations were based on the interaction of Kuo and Herling [2] and its modified version [11]. They were successful in describing the energy spectrum of the nuclei in the vicinity of ^{208}Pb as well as in describing the static magnetic moments of some of the isomeric states of these nuclei. Successful calculations were performed for ^{208}Po and ^{209}Po nuclei [14,15] using the residual interaction derived by means of the $\hat{Q}$ box folded-diagram approach [16,17] which uses the CD-Bonn nucleon-nucleon potential [18] renormalized by the $V_{\text{low-}k}$ approach [4]. Such an approach was also used to derive the H208 interaction for the nuclei northeast of ^{208}Pb [19,20]. The calculations with this interaction describe well both the energy spectrum and the available electromagnetic properties of the nuclei from the region. One highlight of the H208 calculations is that they could account for the experimentally observed isovector character of the 2_2^+ state in ^{212}Po [21]. Recent measurement of the lifetime of the 2_1^+ state in ^{212}Po by Kocheva *et al.* [22], however, revealed that the shell model overestimates the transition probability of the $2_1^+ \rightarrow 0_1^+$ transition significantly. Such behavior was also observed in the neighboring ^{210}Po. This was ascribed to the neglect of particle-hole excitations of high order in the wave function of the ground state of these nuclei [11,23]. Aside from this problem, the shell-model description of the transitions between the low-lying states in ^{210}Po is very good. Overall, the shell-model calculations also describe the available experimental data for the low-lying states of ^{212}Po with an exception of the $2_1^+ \rightarrow 0_1^+$ transition.

The ^{212}Po nucleus has been also discussed actively in terms of a α-clusterization. The main motivation for this approach is the very large α-decay width of the ground state which could be described by including α-cluster components in the wave function [24–28]. However, such an approach applied to the higher lying states yields only a quantitative description of the observed structure. It has been stated by Ohkubo [28] that it could be expected that the α-cluster structure is destroyed by the increase of the mixing of the shell-model components

*Present address: TRIUMF, 4004 Wesbrook Mall, Vancouver, BC V6T 2A3, Canada

due to the spin-orbit interaction which increases with the spin of the state. On the other hand, several negative parity states have been disused in terms of '$\alpha + {}^{208}$Pb' cluster structure based on the strongly enhanced $E1$ transitions stemming from those states. However, a very recent high-intensity γ-γ measurement has suggested that those states may, in fact, have positive parity and could be interpreted within the shell model without the need for α clustering [29]. During the preparation of this paper, new experimental data on the lifetimes of the 4_1^+ and 6_1^+ became available [30]. The authors of Ref. [30] have also employed α-clustering model calculations. While the calculations reproduce the $B(E2; 2_1^+ \rightarrow 0_1^+)$ well, the agreement for the higher-lying states is not satisfactory, especially for $B(E2; 4_1^+ \rightarrow 2_1^+)$. Additionally, these calculations overestimate significantly the observed low α branching of the yrast states [31]. While the necessity to include α-cluster components in the wave function of the ground state (g.s.) is clear, the situation for the higher lying states is not completely understood.

In the present study, independent results for the lifetimes of the first excited 4^+ and 6^+ states in ^{212}Po are presented. The structure of the low-lying yrast band is discussed with shell-model calculations done using the H208 interaction.

II. EXPERIMENT AND ANALYSIS

The ^{212}Po nuclei were populated via the ^{208}Pb(^{18}O, ^{14}C)^{212}Po α-transfer reaction. The ^{18}O beam of energy 85 MeV was provided by the FN-TANDEM accelerator at the University of Cologne. The target was a 0.8 mg/cm^2 ^{208}Pb layer with 99.14% isotopic enrichment evaporated on 0.4 mg/cm^2 Mg support foil and was placed inside the Cologne plunger device [32], where the Mg was facing the beam. A 1.7 mg/cm^2 Mg foil used to stop the ejected ^{212}Po nuclei was stretched parallel to the target. The γ rays produced in the experiment were detected by an array of 11 HPGe detectors placed in two rings at 45° and 142° around the target chamber. Recoiling ions were detected by an array of six photovoltaic pin diodes, placed at backward angles, covering angles between 120° and 165°. These detectors serve for a selection of the different transfer reactions induced on the target and the stopper. Due to the large mass difference of the target and stopper the transfer reactions induced on the target and the stopper are well separated. Additionally, the detectors also restrict the reaction geometry, resulting in better separation between the shifted and the unshifted components in the γ-ray spectrum. Data were taken at 11 target-to-stopper distances, raging from 12 μm to 911 μm. These distances were determined relative to a electrical contact of the foils obtained via the capacitance method [32,33] and were kept constant by the active feedback system of the Cologne plunger device [32]. The γ singles particle-gated spectrum for the shortest distance of 12 μm is displayed in Fig. 1(a). Due to the clean particle gate, the obtained spectrum contains almost exclusively transitions belonging to the nucleus of interest. These transitions are indexed and the information on them is summarized in Table I. The intensities of the transitions were measured in the singles spectrum using integration.

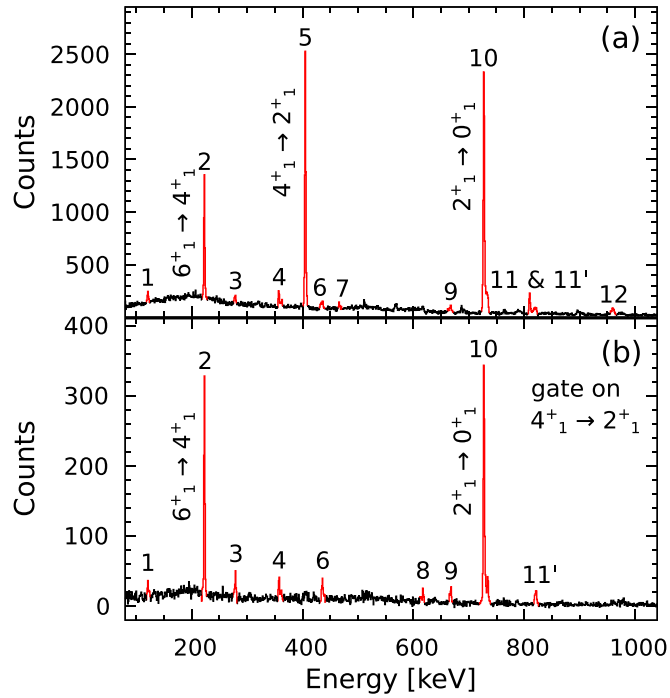

FIG. 1. (a) Particle-gated singles γ-ray spectrum of the forward detector ring taken at the shortest distance of 12 μm. The transitions belonging to ^{212}Po are indicated and colored in red. A list of the transitions is given in Table I. (b) Particle-γ gated γ-ray spectrum for all the distances of the forward detector ring.

Some of the transitions appear as doublets in the γ singles spectrum. Their intensities were measured using a proper γ-γ coincidence spectrum, taking into account the detector efficiency. Using γ-γ coincidence analysis a level scheme relevant for this experiment was built and is displayed in Fig. 2.

TABLE I. γ-ray transitions observed in the ^{208}Po(^{18}O, ^{14}C)^{212}Po reaction. Transition intensities are normalized to the $2_1^+ \rightarrow 0_1^+$ transition. The spin assignments and the energies of the transitions are taken from the evaluated Nuclear Data Sheet [31], Ref. [34], and this experiment.

Index	Transition	Energy [keV]	Intensity
1	$8_1^+ \rightarrow 6_1^+$	121	2.0(2)
2	$6_1^+ \rightarrow 4_1^+$	223	21.1(4)
3	$(8_1^-) \rightarrow 8_1^+$	276	2.6(5)
4	$10_1^+ \rightarrow 8_1^+$	357	3.7(4)
5	$4_1^+ \rightarrow 2_1^+$	405	57.6(8)
6	$(6_1^-) \rightarrow 6_1^+$	433	3.8(6)
7	$4_2^{(-)} \rightarrow (3_1^-)$	466	3.3(12)
8	$(4_1^-) \rightarrow 4_1^+$	612	~1
9	$(6) \rightarrow 6_1^+$	662	3.5(14)
10	$2_1^+ \rightarrow 0_1^+$	727	100.0(12)
11	$(3_1^-) \rightarrow 2_1^+$	810	13.3(20)
11'	$(4) \rightarrow 4_1^+$	813	~2
12	$2_3^+ \rightarrow 2_1^+$	952	6.4(12)
—	$2_3^+ \rightarrow 0_1^+$	1680	3.8(6)

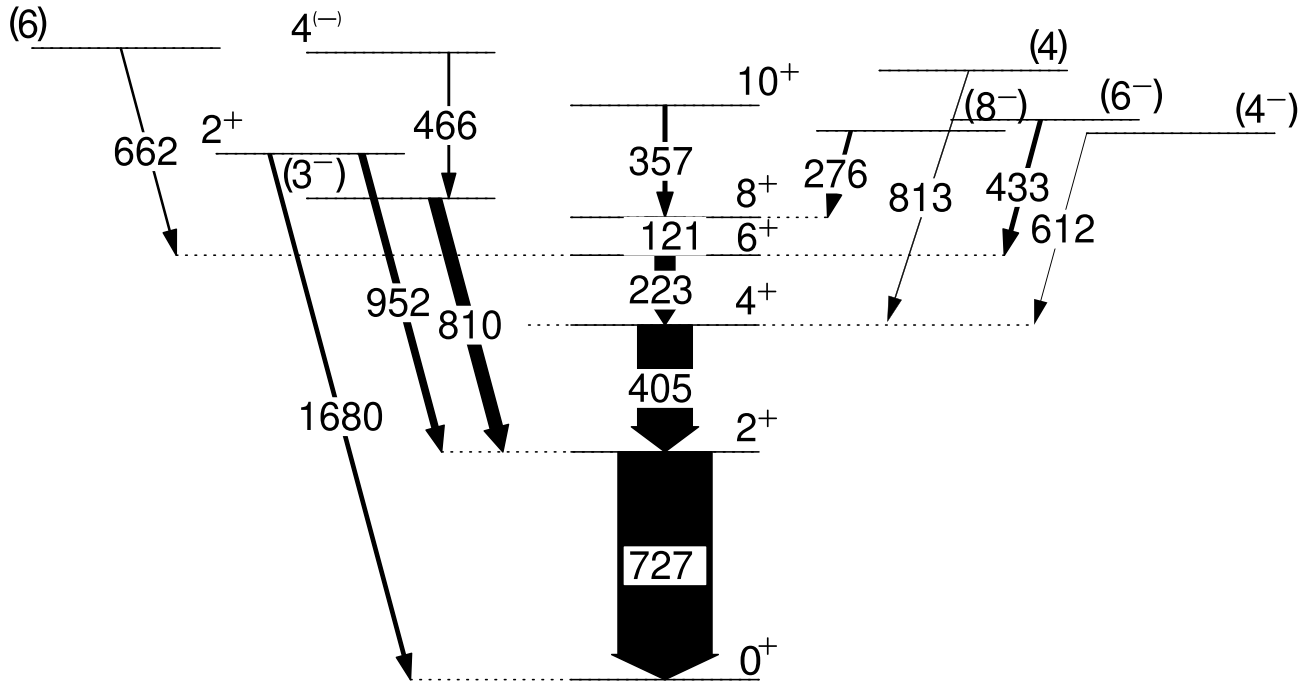

FIG. 2. Level scheme of ^{212}Po populated in the ^{208}Po(^{18}O, ^{14}C)^{212}Po reaction. The width of the arrows is proportional to the observed γ-ray intensity of the transitions, which are given in Table I.

A. The lifetime of the 4_1^+ state

The lifetime of the 4_1^+ state was determined using the recoil-distance Doppler-shift (RDDS) method [32,35,36]. In this method the the lifetime of the state of interest is determined by using the the quantity $R(t)$ which is defined as $R(t) = I_u(t)/(I_u(t) + I_s(t))$, where $I_s(t)$ and $I_u(t)$ are the intensity of the shifted and the unshifted components of a transition which decays the excited state of interest. The ratio $R(t)$ is known as the decay curve and depends on the time of flight of the excited ions between the target and the stopper. In the most simple case where only one state is populated in a nuclear reaction and there is no feeding coming from high-lying states the decay cure is a simple exponent. In a realistic case, the feeding coming from the higher-lying state is taken into account by solving a system of differential equations known as the Bateman equations [32]. The average speed of $v = 1.15(5)\%$ c of the ejected ^{212}Po nuclei was determined by measuring the Doppler shift of several of the strongest transitions observed in the experiment. This speed was used to calculate the average time of flight between the target and the stopper. When using the Bateman equations only the lifetime of the 4_1^+ state was used as a fit variable. All other parameters, i.e., the lifetime of the states feeding the 4_1^+ state and their intensities were fixed. To illustrate the feeding of the 4_1^+ state a spectrum gated on the $4_1^+ \rightarrow 2_1^+$ transition is displayed in Fig. 1(b). From this figure and the level scheme given in Fig. 2, it could be seen that the only feeding of the 4_1^+ state is coming from the 6_1^+ state via the $6_1^+ \rightarrow 4_1^+$ transition and from the states at 1744.9 keV and 1945.8 keV via the 612 keV and 813 keV transitions, respectively. The feeding via the 6_1^+ state is easily accounted for as the lifetimes of the 6_1^+ and its feeders are known [31]. In the analysis the lifetime of the 6_1^+ state is taken as 1.65(15) ns, which is measured in this experiment (see next section). The two other direct feeding contributions are fast as initial states both have lifetime of 0.48(14) ps [31]. To obtain the $R(t)$ ratios, the shifted and the unshifted components of the $4_1^+ \rightarrow 2_1^+$ γ-ray transition were fitted for each distance using two Gaussian functions. The widths of the Gaussian functions, different for the two components, and their respective positions were kept constant during the fit for each of the distances in order to minimize possible systematic errors. The uncertainties of the ratios include the statistical error and the systematic uncertainty that arise when varying the various fit parameters. The fits to the spectra for three representative distances for the forward detector ring are displayed in Fig. 3. The Bateman fit to the measured $R(t)$ values is displayed in Fig. 3(d).

To obtain the uncertainty of the measured lifetime a Monte Carlo simulation was performed. All the input parameters used in the fit are independently varied within the corresponding experimental uncertainties before performing the fit. This process is repeated one million times and the results from the fits are written in a histogram which is displayed in Fig. 3(e). The distribution is almost symmetric, with a very small sloping towards the higher lifetimes. In this case the uncertainty of the lifetime is defined simply as the standard deviation of these values. The result for the lifetime of the 4_1^+ state measured using the forward detector ring is $\tau_f = 100(9)$ ps. A similar procedure performed for the backward detector rings yields a lifetime $\tau_b = 103(10)$ ps. The corresponding figures are displayed in Fig. 3(f–j). The results for both detector rings coincided very well with each other and the final result of $\tau = 101(7)$ ps is adopted as the weighted average of these two values. The final uncertainty combination of statistical.

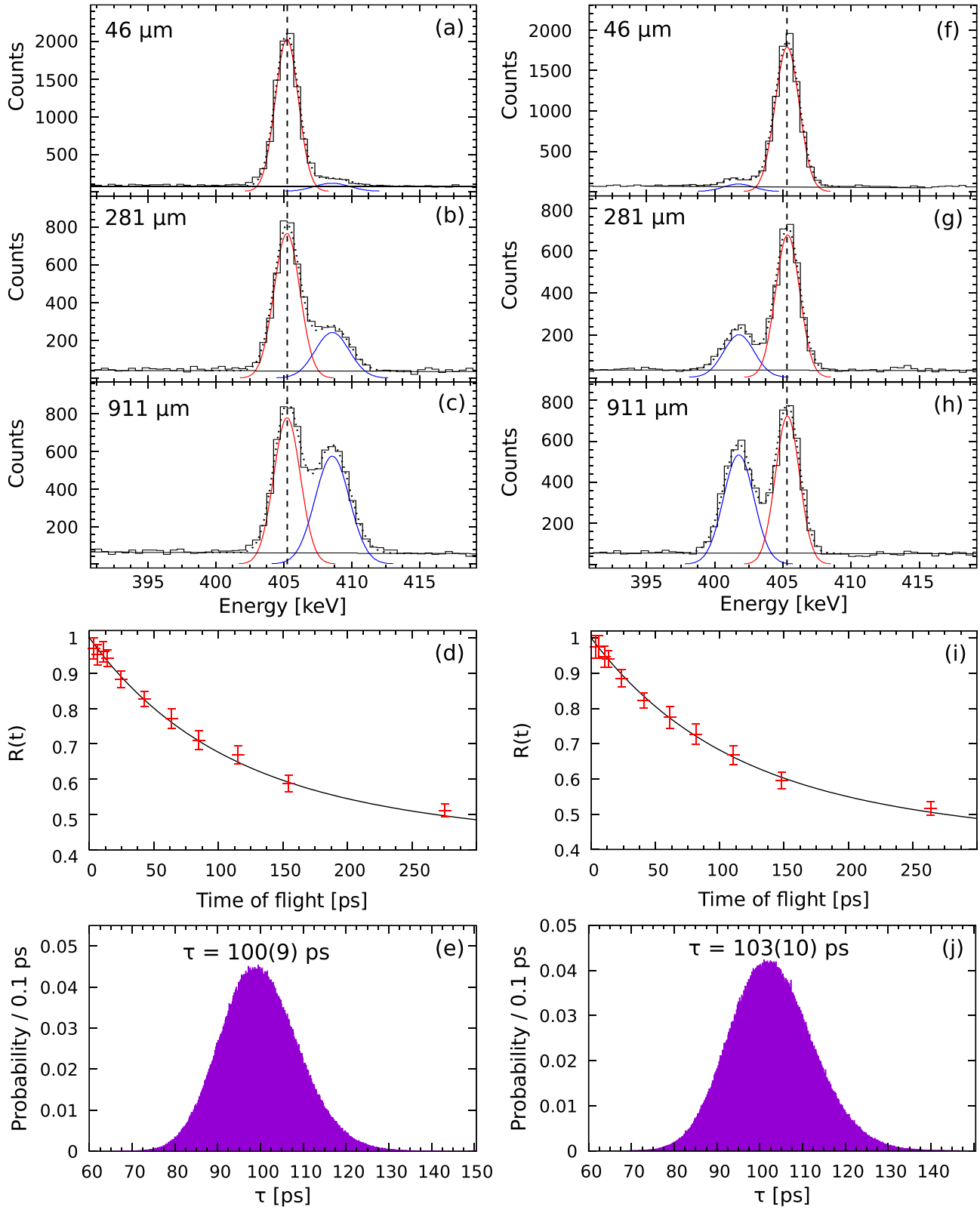

FIG. 3. (a,b,c) Fits to the $4_1^+ \rightarrow 2_1^+$ transition (dotted black line) of the forward-detector ring for three distances used to determine the intensity of the shifted (blue solid line) and the unshifted components (red solid line). The dashed horizontal line indicates the 405 keV energy of the unshifted component of the $4_1^+ \rightarrow 2_1^+$ transition. The black solid line is the background parametrization. (d) The Bateman fit to the obtained $R(t)$ of the $4_1^+ \rightarrow 2_1^+$ transition for all distances used to determine the lifetime of the 4_1^+ state. (e) Probability distribution for the lifetime obtained using a Monte Carlo simulation as explained in the text, used to the determined the uncertainty of the measured lifetime. (f–j) Same as (a–e) but for the backward detector ring.

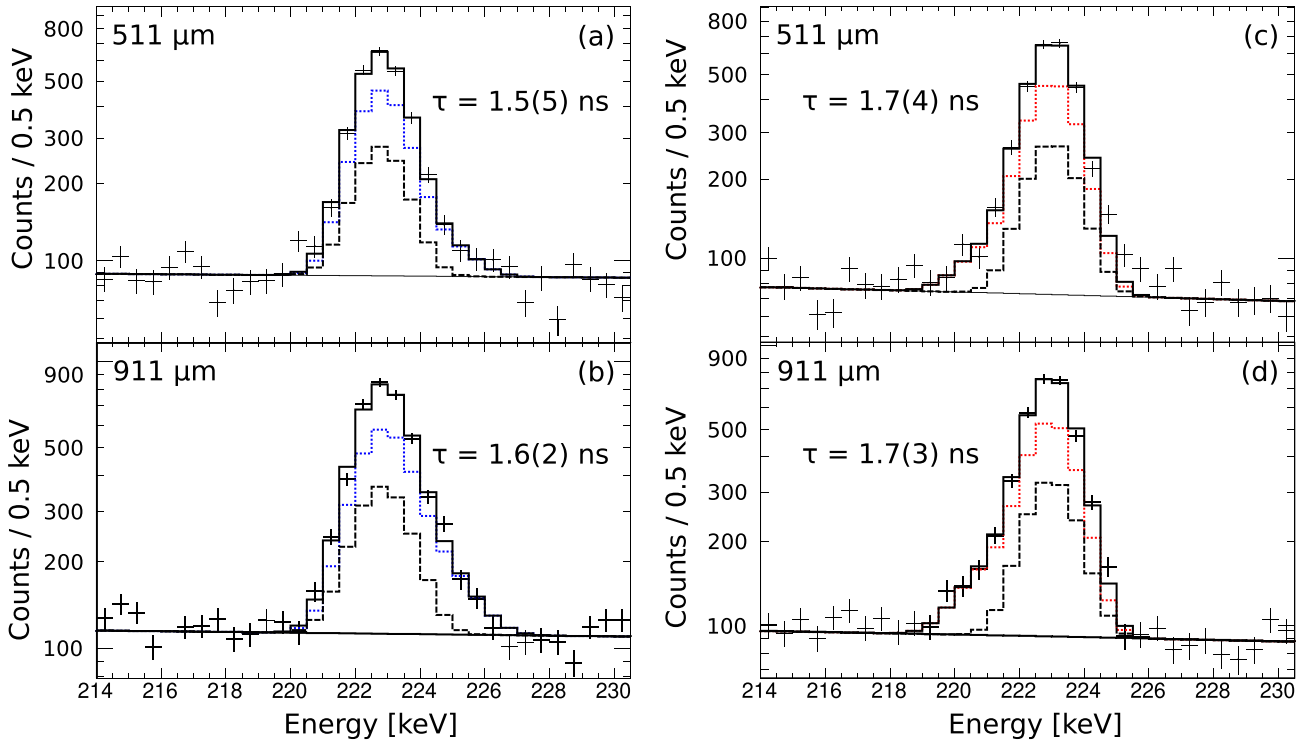

FIG. 4. (a) DSA fit to the spectrum of the $6_1^+ \rightarrow 4_1^+$ transition of the forward detector ring for target-to-stopper distance of 511 μm used to determine the lifetime of the 6_1^+ state. The black solid straight line is the background parametrization, the dashed black peak represents the long-lived feeding from the 8_1^+ state, the blue dotted line is the DSA fit to the spectrum excluding the long-lived feeding and the solid black line is the sum of the both spectra. Please note, that the y scale is logarithmic. (b) Same as (a) but for the target-to-stopper distance of 911 μm. (c) and (d) same as (a) and (b) but for the backward detector ring and the line representing the fit excluding the long-lived feeding is red.

This result is consistent with the value of 100(14) ps obtained in a fast-timing measurement performed in Ref. [30].

B. The lifetime of the 6_1^+ state

The lifetime of the first excited 6^+ state is long and is on the limit of applicability of the RDDS method. The major problem in applying directly this method is the lack of knowledge of the width of the shifted component of the $6_1^+ \rightarrow 4_1^+$ transition, which has a significant influence on the measured lifetime. To obtain the lifetime of the 6_1^+ state, a simulation similar to the ones used when determining the lifetimes of excited states using Doppler-shift attenuation (DSA) method was performed. This simulation was performed in the framework of the computer code APCAD [37]. The slowing process of the ions in the target and the stopper as well as the drift in the vacuum between them is modeled by a Monte Carlo simulation using the toolkit GEANT4 [38]. The electronic and nuclear stopping powers used in the simulation are provided externally and are taken from SRIM [39]. The doubly differential cross section of the ^{208}Pb(^{18}O, ^{14}C)^{212}Po reaction, which defines the geometry of the reaction, was estimated using the GRAZING code [40,41]. After the individual traces of the ions are simulated, their γ-ray spectrum is projected on detectors. In the procedure, APCAD takes into account the geometrical restrictions imposed by the solar cells and the response of the HPGe detectors. This calculated spectrum is then fitted to the experimental one using only the lifetime of the 6_1^+ state as a fit variable. The feeding coming from the 8_1^+ state which has a lifetime of 21.06(43) ns [31] is taken into account when performing the fit. Any other long-lived components can be excluded as the feeding coming from the 6_1^- and 6_2^- states is fast. The only sensitive distances for this relatively long lifetime are the longest two distances of 511 μm and 911 μm. The fits to the experimental data and the results for these distances for both the forward and the backward detector rings are displayed in Fig. 4. The final result for the lifetime of 6_1^+ state $\tau = 1.65(15)$ ns is taken as the weighted average of the individual results. This result is considerably longer than the adopted value of 1.1(3) ns [42] but agrees well with the very recently measured value of 1.66(28) ns [30]. Moreover, using this lifetime in the RDDS analysis for the lifetime of the 4_1^+ state yields a much better description of the decay curve at long distances.

Using the measured lifetimes and the α-decay branching and conversion coefficient given in Ref. [31], the reduced transition probabilities of the $4_1^+ \rightarrow 2_1^+$ and $6_1^+ \rightarrow 4_1^+$ transitions were calculated. These results are summarized in Table II together with other experimentally available reduced transition probabilities in ^{212}Po which are discussed in the next section.

III. DISCUSSION

The newly acquired experimental data is compared to large-scale shell-model calculations performed using the orbitals $0h_{9/2}$, $1f_{7/2}$, $0i_{13/2}$, $1f_{5/2}$, $2p_{3/2}$, and $2p_{1/2}$ for the

TABLE II. Experimental and calculated (SM) excitation energies and reduced $E2$ transition probabilities in ^{212}Po. Experimental data is taken from the evaluated nuclear data sheets [31] and this experiment.

	E_x (MeV)			$B(E2; J_i \to J_f)(e^2\text{fm}^4)$		
J_i^π	Experiment	SM	J_f^π	Experiment	SM[a]	SM[b]
2_1^+	0.727	0.730	0_1^+	193^{+26}_{-22}	617	402
4_1^+	1.133	1.156	2_1^+	700^{+52}_{-45}[c]	735	473
6_1^+	1.355	1.368	4_1^+	677^{+68}_{-56}[c]	531	332
8_1^+	1.475	1.431	6_1^+	342(9)	272	168
2_2^+	1.513	1.460	0_1^+	29(4)	43	64
			2_1^+	24(16)	12	14

[a]Using $e_p = 1.5e$ and $e_n = 0.85e$.
[b]Using $e_p = 1.5e$ and $e_n = 0.5e$.
[c]This work.

protons and the $1h_{9/2}$, $0i_{11/2}$, $1h_{7/2}$, $2d_{5/2}$, $2d_{3/2}$, $3s_{1/2}$, and $0j_{15/2}$ for the neutrons taken above the ^{208}Pb doubly magic core. The calculations are performed using the very recently developed H208 interaction [19,20]. The detailed procedure of deriving the H208 interaction is given in Refs. [19,20]. The interaction is obtained from the CD-Bonn nucleon-nucleon potential [18] by applying a $V_{\text{low-}k}$ cutoff procedure [4,5]. The interaction is then adapted to the model space by $\hat{\text{Q}}$ box folded-diagram approach [5,43]. Some monopole adjustments are made to the effective two-body forces in order to mimic three-body forces as suggested in Ref. [44].

As already mentioned in Ref. [20], the calculated energy levels for many of the even-even nuclei close to the ^{208}Pb core show an excellent agreement with the experimental data. This is also the case for the ^{212}Po nucleus as shown numerically in Table II and schematically in Fig. 5. Within the yrast band, the agreement is particularly good as the 2_1^+, 4_1^+, 6_1^+ states are only slightly overestimated with less than 25 keV difference to the experimental values. The deviation for the 8_1^+ state is slightly larger, but the agreement is still good. The excitation energy of the off-yrast 2_2^+ state is also described well. Here it is worth mentioning that the wave-function character of the yrast 0^+–8^+ and the 2_2^+ states is dominated by the configuration $\pi h_{9/2}^2 \otimes \nu 1g_{9/2}^2$. Indeed, it was demonstrated in Ref. [22] that a qualitative description of the excited states of ^{212}Po could be achieved in the framework of a single-j shell-model calculations using the $\pi h_{9/2}^2$ and the $\nu 1g_{9/2}^2$ configurations.

The first step in the calculation of the electromagnetic decay rates is to fix the effective operators. The scarcity of experimental data makes this task very difficult. In the present work, the shell-model calculations are performed using two sets of effective charges: ($e_p = 1.5e$ and $e_n = 0.85e$), the same as the ones used in Ref. [17], and the standard ones ($e_p = 1.5e$ and $e_n = 0.5e$), which is consistent with the values usually employed in this space [20]. The calculated values are given in Table II, together with the available experimental data. The results for the first set of effective charges are also given schematically in Fig. 5. This set of effective charges reproduces very well the observed reduced transition probabilities with $B(E2; 4_1^+ \to 2_1^+)$ and $B(E2; 8_1^+ \to 6_1^+)$ lying within the experimental uncertainty. The off-yrast transition probabilities $B(E2; 2_2^+ \to 2_1^+)$ and $B(E2; 2_2^+ \to 0_1^+)$ are also described acceptably well. However, the known problem for the $B(E2; 2_1^+ \to 0_1^+)$ transition rate still persists, with the calculation overestimating the experimental value more than three times (cf. Table II). The good agreement for the $B(E2; 4_1^+ \to 2_1^+)$ indicates that the shell-model calculations describe the wave function of the 2_1^+ state. The problem with the $B(E2; 2_1^+ \to 0_1^+)$ is most probably in the wave function of the ground state, influenced by additional contributions which could not be described by the shell model. In the case of the neighboring ^{210}Po nucleus, it has been argued that these contributions are of particle-hole type [11,23] which are not taken into account due to the choice of the model

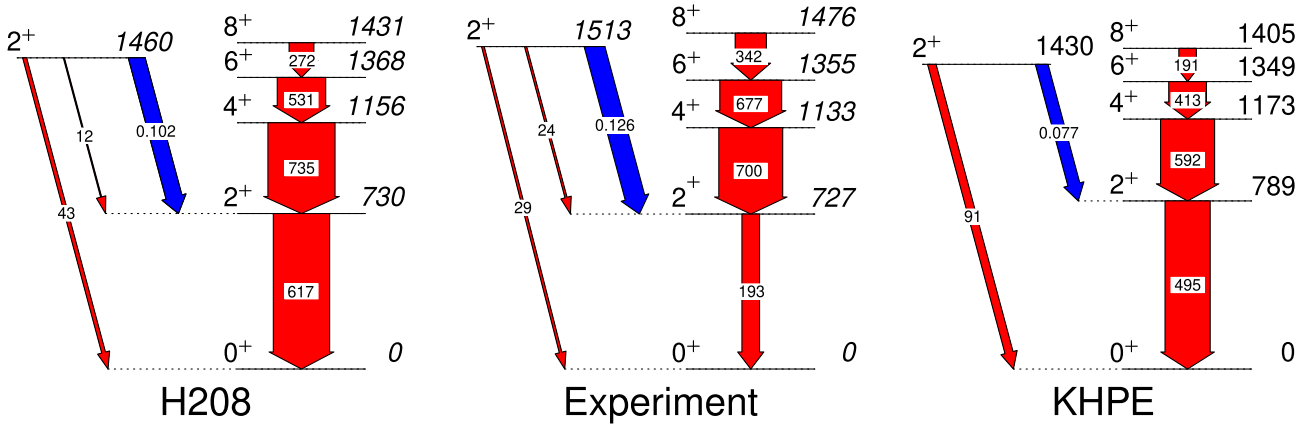

FIG. 5. Comparison of experimental low-lying excited states of ^{212}Po (middle) with the shell-model calculations performed using the H208 interaction (left) and the KHPE interaction (right). See text for details of the calculations. Experimental data are taken from the evaluated nuclear data sheets [31] or this experiment. The energies of the levels are given in keV. The width of the red arrows are proportional to the absolute $E2$ transition strengths between the states. The numbers over the red arrows are the reduced $E2$ transition probabilities in $e^2\text{fm}^4$. The blue arrows represent the $M1$ transitions. The reduced $M1$ transition probabilities are given in μ_N^2. The positions of the 8^+ states have been elevated by 100 keV to make the transition arrows to the 6_1^+ state clearly visible.

space which does not allow particle-hole excitations across the major closed shells. For ^{212}Po, altogether, with an exception of the $2_1^+ \rightarrow 0_1^+$ transition, the shell-model transition rates follow the behavior of experimental ones, in particular their decrease toward the 8_1^+ state, independent of the choice of the effective charges. This fact, together with the good description of the energy spectrum, proves the ability of the shell model to describe the spectroscopic properties of the excited states of ^{212}Po.

The H208 calculations also describe well the observed relatively high $B(M1)$ transition rate between the 2_2^+ and 2_1^+ states, where the calculations predict a $M1$ transition strength of 0.102 μ_N^2 [20] while the experimental value is 0.126(16) μ_N^2 [21]. The character of the $2_{1,2}^+$ states, investigated in detail in Refs. [20,29], reveals the isovector character of the 2_2^+ state, which explains the enhanced $B(M1; 2_2^+ \rightarrow 2_1^+)$ values. In particular, it was shown that the 2_1^+ and 2_2^+ wave functions comprise a significant component of the fully symmetric and mixed-symmetry states, respectively.

For comparison, we have also performed large-scale shell-model calculations using the modified Kuo-Herling interaction (abbreviated as KHPE) [11] which is often used for nuclei in the region northeast of ^{208}Po. The calculations were carried out in the same model space as the one used in the H208 calculations and using the same effective charges ($e_p = 1.5e$ and $e_n = 0.85e$) and the gyromagnetic ratios from Refs. [20,29]. The results are presented in Fig. 5. It could be seen that the calculations carried out with the KHPE interaction also provide a generally good description of the low-energy structure of ^{212}Po. Please note that by increasing e_n, the transition probabilities could be brought to a better agreement with the experimental data. However, the H208 interaction provides a better description of the excitation spectrum and describes better the $E2$ transition strengths from the 2_2^+ state. A comparison between the two interactions for the higher-lying states can be found in Ref. [29] and a more general comparison for the nuclei in the region can be found in Ref. [19].

IV. CONCLUSION

The lifetimes of the first excited 4^+ and 6^+ states in ^{212}Po were measured using the RDDS technique. The deduced reduced transition probabilities were compared to large-scale shell-model calculations done using the recently developed H208 interaction. The calculations describe very well both the energy spectrum and the electromagnetic transition properties of the observed low-lying nuclear structure including the properties of the isovector 2_2^+ state with the only exception being the $2_1^+ \rightarrow 0_1^+$ transition. This shows that with a proper interaction the ^{212}Po nucleus could be well described by the shell model without the need of α clustering. Only the wave function of the ground state of ^{212}Po has additional contributions, outside the shell model. Most probably these contributions are associated with α clustering which could intuitively be expected as the ground state has a very large α-decay width.

ACKNOWLEDGMENTS

V.K. acknowledges the support by the Bulgarian Ministry of Education and Science under the National Research Program Young scientists and postdoctoral students and the financial support of NSCRC. A.E. acknowledge the support by the BMBF under Grant No. 05P21PKFN1. This work was supported by the DAAD partnership agreement between the University of Cologne and University of Sofia. The help of the Cologne Tandem accelerator operators for providing the beam is acknowledged.

[1] M. G. Mayer, Phys. Rev. **78**, 16 (1950).
[2] G. H. Herling and T. T. S. Kuo, Nucl. Phys. A **181**, 113 (1972).
[3] T. Hamada and I. D. Johnson, Nucl. Phys. **34**, 382 (1962).
[4] S. Bonger, T. T. S. Kuo, and L. Coraggio, Nucl. Phys. A **684**, 432 (2001).
[5] M. Hjorth-Jensen, T. T. S. Kuo, and E. Osnes, Phys. Rep. **261**, 125 (1995).
[6] R. Machleidt, K. Holinde, and Ch. Elster, Phys. Rep. **149**, 1 (1987).
[7] D. R. Entem and R. Machleidt, Phys. Rev. C **68**, 041001(R) (2003).
[8] R. B. Wiringa, V. G. J. Stoks, and R. Schiavilla, Phys. Rev. C **51**, 38 (1995).
[9] J. B. McGrory and T. T. S. Kuo, Nucl. Phys. A **247**, 283 (1975).
[10] T. R. McGoram, G. D. Dracoulis, A. P. Byrne, A. R. Poletti, and S. Bayer, Nucl. Phys. A **637**, 469 (1998).
[11] E. K. Warburton and B. A. Brown, Phys. Rev. C **43**, 602 (1991).
[12] L. Coraggio, A. Covello, A. Gargano, N. Itaco, and T. T. S. Kuo, Phys. Rev. C **58**, 3346 (1998).
[13] E. Caurier, M. Rejmund, and H. Grawe, Phys. Rev. C **67**, 054310 (2003).
[14] D. Kalaydjieva, D. Kocheva, G. Rainovski, V. Karayonchev, J. Jolie, N. Pietralla, M. Beckers, A. Blazhev, A. Dewald, M. Djongolov, A. Esmaylzadeh, C. Fransen, K. A. Gladnishki, A. Goldkuhle, C. Henrich, I. Homm, K. E. Ide, P. R. John, R. Kern, J. Kleemann *et al.*, Phys. Rev. C **104**, 024311 (2021).
[15] V. Karayonchev, M. Stoyanova, G. Rainovski, J. Jolie, A. Blazhev, M. Djongolov, A. Esmaylzadeh, C. Fransen, K. Gladnishki, L. Knafla, D. Kocheva, L. Kornwebel, J.-M. Régis, G. De Gregorio, and A. Gargano, Phys. Rev. C **103**, 044309 (2021).
[16] L. Coraggio, A. Covello, A. Gargano, N. Itaco, and T. T. S. Kuo, Prog. Part. Nucl. Phys. **62**, 135 (2009).
[17] L. Coraggio, A. Covello, A. Gargano, N. Itaco, and T. T. S. Kuo, Ann. Phys. (NY) **327**, 2125 (2012).
[18] R. Machleidt, Phys. Rev. C **63**, 024001 (2001).
[19] H. Naïdja, Phys. Scr. **94**, 014005 (2019).
[20] H. Naïdja, Phys. Rev. C **103**, 054303 (2021).
[21] D. Kocheva, G. Rainovski, J. Jolie, N. Pietralla, C. Stahl, P. Petkov *et al.*, Phys. Rev. C **93**, 011303(R) (2016).
[22] D. Kocheva, G. Rainovski, J. Jolie, N. Pietralla, A. Blazhev, R. Altenkirch *et al.*, Phys. Rev. C **96**, 044305 (2017).

[23] V. Karayonchev, A. Blazhev, A. Esmaylzadeh, J. Jolie, M. Dannhoff, F. Diel, F. Dunkel, C. Fransen, L. M. Gerhard, R.-B. Gerst, L. Knafla, L. Kornwebel, C. Müller-Gatermann, J.-M. Régis, N. Warr, K. O. Zell, M. Stoyanova, and P. Van Isacker, Phys. Rev. C **99**, 024326 (2019).
[24] K. Varga, R. G. Lovas, and R. J. Liotta, Phys. Rev. Lett. **69**, 37 (1992).
[25] F. Hoyler, P. Mohr, and G. Staudt, Phys. Rev. C **50**, 2631 (1994).
[26] B. Buck, A. C. Merchant, and S. M. Perez, Phys. Rev. Lett. **72**, 1326 (1994).
[27] B. Buck, J. C. Johnston, A. C. Merchant, and S. M. Perez, Phys. Rev. C **53**, 2841 (1996).
[28] S. Ohkubo, Phys. Rev. Lett. **74**, 2176 (1995).
[29] A. Fernández *et al.*, Phys. Rev. C **104**, 054316 (2021).
[30] Ma. von Tresckow, M. Rudigier, T. M. Shneidman, Th. Kröll, M. Boromiza, C. Clisu, C. Costache, D. Filipescu, N. M. Florea, I. Gheorghe, K. Gladnishki, A. Ionescu, D. Kocheva, R. Lică, N. Mărginean, R. Mărginean, K. R. Mashtakov, C. Mihai, R. E. Mihai, A. Negret *et al.*, Phys. Lett. B **821**, 136624 (2021).
[31] K. Auranen and E. A. McCutchan, Nucl. Data Sheets **168**, 117 (2020).
[32] A. Dewald, O. Möller, and P. Petkov, Prog. Part. Nucl. Phys. **67**, 786 (2012).
[33] T. K. Alexander and A. Bell, Nucl. Instrum. Methods **81**, 22 (1970).
[34] A. Astier, P. Petkov, M.-G. Porquet, D. S. Delion, and P. Schuck, Eur. Phys. J. A **46**, 165 (2010).
[35] D. B. Fossan and E. K. Warburton, *Nuclear Spectroscopy and Reactions, Part C*, Pure and Applied Physics (Elsevier, 1974), Vol. 40 p. 307.
[36] P. J. Nolan and J. F. Sharpey-Schafer, Rep. Prog. Phys. **42**, 1 (1979).
[37] C. Stahl, J. Leske, M. Lettmann, and N. Pietralla, Comput. Phys. Commun. **214**, 174 (2017).
[38] S. Agostinelli *et al.*, Nucl. Instrum. Methods Phys. Res. A **506**, 250 (2003).
[39] J. F. Ziegler, M. D. Ziegler, and J. P. Biersack, Nucl. Instrum. Methods Phys. Res. B **268**, 1818 (2010).
[40] A. Winther, Nucl. Phys. A **572**, 191 (1994).
[41] R. Yanez and W. Loveland, Phys. Rev. C **91**, 044608 (2015).
[42] A. R. Poletti, G. D. Dracoulis, A. P. Byrne, and A. E. Stuchbery, Nucl. Phys. A **473**, 595 (1987).
[43] K. Suzuki and S. Y. Lee, Prog. Theor. Phys. **64**, 2091 (1980).
[44] A. P. Zuker, Phys. Rev. Lett. **90**, 042502 (2003).